Title:

Separation and enrichment of sodium-motile bacteria using cost-effective microfluidics.

Authorship:

Jyoti P Gurung[1], Moein Navvab Kashani[2,3], Sanaz Agarwal[1], Murat Gel[4,5], Matthew AB Baker[1,5].

1. School of Biotechnology and Biomolecular Science, UNSW Sydney
2. Future Industries Institute, University of South Australia, Mawson Lakes, SA 5095
3. Australian National Fabrication Facility – South Australia Node, Mawson Lakes, SA 5095
4. CSIRO Manufacturing, Clayton
5. CSIRO Future Science Platform for Synthetic Biology

correspondence: matthew.baker@unsw.edu.au

Abstract

Many motile bacteria are propelled by the rotation of flagellar filaments. This rotation is driven by a membrane protein known as the stator-complex, which drives the rotor of the bacterial flagellar motor. Torque generation is powered in most cases by proton transit through the stator complex, with the next most common ionic power source being sodium. Synthetic chimeric stators which combine sodium- and proton-powered stators have enabled the interrogation of sodium-stators in species that are typically proton-powered, such as the sodium powered PomA-PotB stator complex in *E. coli.* Much is known about the signalling cascades that respond to attractant and govern switching bias as an end-product of chemotaxis, however less is known about how energetics and chemotaxis interact to affect the colonisation of environmental niches where ion concentrations and compositions may vary. Here we designed a fluidics system at low cost for rapid prototyping to separate motile and non-motile populations of bacteria. We measure separation efficiencies at varying ionic concentrations and confirm using fluorescence that our device can deliver eight-fold enrichment of the motile proportion of a mixed population of motile and non-motile species. Furthermore, our results show that we can select bacteria from reservoirs where sodium is not initially present. Overall, this technique can be used to implement long-term selection from liquid culture for directed evolution approaches to investigate the adaptation of motility in bacterial ecosystems.

Introduction

Halophilic, or salt-loving, microorganisms are predominantly found in salt-enriched habitats such as in the deep sea. One of the bacterial phenotypes that is directly influenced by the presence or absence of ionic salts such as sodium is bacterial motility (1) Sodium-motility has particular medical relevance since pathogens such as *Vibrio cholerae*, which has up to 4M cases per year, strictly requires sodium ions to drive motility to spread disease (2). Bacterial motility is, for the most part, driven by using a molecular motor called the bacterial flagellar motor (BFM). The BFM is a transmembrane nanomachine powered by cation influx consisting of a rotor, attached to a long filamentous protrusion known as a 'flagellum', and membrane-bound stator complexes that act as ion porters that couple ion transit to torque generation (3). Bacteria navigate in their surrounding medium by controlling when they change directions of rotating flagella, either clockwise or anticlockwise, to drive motility in a foraging search for nutrient, or to avoid repellents (4). The development of more efficient and cost-effective techniques to separate these bacteria with larger precision enables us to examine subtle differences in bacterial phenotype, in liquid and at high throughput. Microfluidics platforms are emerging as a technology with wide promise for microbiological research and development (5) offering precise control of flow and buffer composition at the micron scales that bacteria inhabit. Microfluidic tools are in widespread use with microscopy platforms and have been

applied to the study and control of gradients which influence motility, such as chemotaxis and thermotaxis, rheotaxis, magnetotaxis and phototaxis (6). Improvements in microfluidics technology now allow fine separation of cells based on subtle differences in motility traits and have applications in synthetic biology (7), directed evolution (8)and applied medical microbiology (9).

In general, microfluidics platform consists of three essential components: (i) syringe pumps to generate flow inside the channel, (ii) a microfluidic chip containing micron-sized channels to direct flow, and (iii) observation and detection methods such as microscopy. Clean-room lithographic fabrication of channel moulds can be expensive, as are commercial microfluidic pumps. Recently cost-effective alternatives such as 3D printed microfluidic devices have been gaining more interest (10). However, 3D printing of microfluidic channels with high spatial resolution and channel smoothness needs further development to completely replace standard method of microfabrication (11). In addition, commercial pumps can be replaced by custom-built syringe pumps which are controlled by cheap micro-computers with strong open-source communities such as Arduino (12). Such pumps perform well as demonstrated by comparative study of commercial and Arduino-driven syringe pumps, which has shown no significant difference in pump's performance such as stability of laminar flow (12).

In this paper, we fabricate a simple and cost-effective microfluidics device with Y-shaped millimetre-sized channel. We demonstrate separation, selection and enrichment of sodium-motile bacteria (*Escherichia coli*), using stable laminar-flow of two streams generated by pressure-driven flow. One of the flow streams can be supplied with bacterial sample and the other flow stream is used to collect sodium-motile bacteria that had swum across the interface into the other stream. We characterise the performance of our system in varying sodium concentration and show the enrichment of the motile fraction of a mixed population and compare reconcile our measurements with simulation of active diffusion of sodium and motile and non-motile bacteria.

Results

Fabrication and characterization of microfluidic device

A microfluidics device with Y-shaped channel (Length of 20 mm and width of 10 mm) was fabricated to generate laminar flow, connected to Arduino-based 3D-printed syringe pump and inverted microscope (Fig. 1c). The width of Y-shaped inlet and outlet were asymmetric, thus, one of the channel widths was 1.2 mm and other was 0.8 mm (Fig. 1b). This resulted the offset of 0.3 mm across the Y-axis (or channel width) about the line drawn along the channel length with origin in the mid-point of the main channel (Fig. 1b). Pulling displacement or negative pressure was applied using syringe pump at desired flow rates (Fig. 1b and c). We controlled flow rate by directing the interval time in milliseconds between steps of our stepper motor. Using 1 mL syringes, our Arduino system had a maximum flow rate of 50 µL/min, corresponding to driving the stepper motor at the maximum speed with 7.6 ms interval between steps (Fig S1). Asymmetric geometry (13) and unequal flow rates (14) have been found to reduce the passing of bacteria across the laminar flow interface, and avoid collection of non-motile cells in outlet 2. Thus, the inlets and outlets of the device were arranged with asymmetric geometry in channel width (Fig. 1) and we established a relative flow rate of 2:1 pulling through outlet 1: outlet 2. This ratio can be for the desired selection stringency. We measured the total volume flowed in a set amount of time (1 mL in 2 hours and 15 min in outlet 1) and confirmed that a mean flow rate of 7.4 µL/min in outlet 1 and 3.7 µL/min in outlet 2 was sustained. Flow rates at inlet were equal, confirmed by equal decrement of inlet reservoir's height throughout the experiment, and thus the flow rate inside the channel was assumed to the average of 7.4 and 3.7 µL/min i.e., 5.55 µL/min across each stream (these flow rates for inlets and outlets were used for subsequent numerical simulation).

We characterized the system and stability of laminar flow using red dye to approximate ionic diffusion. Image analysis of 5-minute video after every 30 minutes time interval was recorded near inlet and outlet to measure the stability of the laminar flow interface using red dye (Fig. 2). Fluctuation of red dye was measured as relative distance traversed by red dye away from the interface and was observed to be less than 1% of channel width i.e., ±0.05 mm for both inlets and outlets (Fig. 2).

Separation, selection and enrichment of sodium-motile bacteria

Separation: We prepared two types of bacterial strains; motile and non-motile bacteria to detect the difference in motility based on sodium ion sensitivity using our microfluidic device. One of the strains was transformed with pSHU1234 plasmid (denoted by pSHU) which showed swimming in the presence of sodium ions whereas the other strain with pSHOT plasmid (denoted by pSHOT) did not (SI Fig. 3a). We drove the system for a total run time of 2 hours and 15 minutes to collect 1 mL of solution from outlet 1 and 0.5 mL from outlet 2 (see Methods). After the completion of a fluidic run, the output volumes from both outlets were serially diluted, and plated, and the number of viable colonies was counted from an overnight culture (see Methods). The separation efficiency (unitless) was then measured as the ratio of number of bacteria from outlet 2 to the total number of bacteria from outlet 1 and outlet 2 (i.e., $S_{eff} = N_{o1} / (N_{o1} + N_{o2})$) (14). We observed the separation efficiency of 0.00005±0.00003 for non-motile pSHOT bacteria and 0.001±0.0005 for sodium-powered motile pSHU bacteria (unpaired *t*-test $p < 0.05$). Motile pSHU bacteria which was suspended in 85 mM of Na+ ions (inlet 1) and run against 85 mM of Na+ ions (inlet 2) showed 30 times more separation than the non-motile pSHOT bacteria (Fig. 3a), confirming the efficacy of our device for separating and distinguishing motile and non-motile *E. coli*. (Fig 3a).

Selection: We then used our device to test the capacity for selection of sodium-sensitive motile bacteria at low sodium concentration by varying the concentration of sodium ions. We loaded bacteria in buffer with no sodium ions (0 mM) (inlet 1) and flowed in against 42.5 mM and 85 mM NaCl to test if diffusion of sodium from the high concentration flow stream (inlet 2) would sufficiently drive rotation of flagella near the interface and enable separation and selection of motile pSHU bacteria. We observed increasing selection efficiency of motile pSHU bacteria with increasing sodium concentration: 0.0003±0.0002 for sodium ion concentration of 42.5 mM and 0.0005±0.0002 for 85 mM NaCl (Fig. 3a). Thus, the number of bacteria separated for 85 mM NaCl was approximately twice that for 42.5 mM NaCl, proportional to the external sodium concentration. Ordinary one-way ANOVA of selected pSHU bacteria in different concentration of Na^+ ion showed separation efficiency was significantly different (p-value <0.05). As a control, we ran bacteria suspended in the buffer with no sodium at all in either of the inlets, which showed no separation for both non-motile pSHOT bacteria and motile pSHU bacteria (SI Fig. 3 – no viable colonies cultured from outlet 2). The increasing selection efficiency of motile bacteria with increasing Na^+ ion concentration is due to diffusion of sodium ions across the interface which was further supported by subsequent numerical simulation.

Enrichment: Finally, after separating and selecting motile bacteria, we used our microfluidic device to enrich sodium-motile bacteria from mixed populations of motile and non-motile bacteria. We fluorescently tagged pSHU motile bacteria with red fluorescent protein DsRed.T4 expressed from DsRed.T4 plasmid and non-motile pSHOT bacteria with green fluorescent protein EGFP (pACGFP1 plasmid) (see materials and method section). To test our capacity to enrichment a subpopulation and measure our enrichment efficiency, we prepared a mixed bacterial sample by mixing red fluorescent, motile, pSHU transformed cells and green fluorescent, non-motile, pSHOT transformed cells in the ratio of 1:1 and 1:9 respectively. We flowed these mixture solutions through our device as per our separation experiments above. The solution collected from outlet 2 after fluidic run was then spread in agar plates to count and measure the enriched ratio of red and green colonies. In spread agar-plate, we observed three types of colonies in term of size and color i.e., large-sized red, small-sized green, and large-sized non-red colonies (SI Fig. 3). We confirmed that those non-red large-sized colonies are motile pSHU bacteria

through sub-culturing on swim plates (SI Fig. 3). We observed that the percentage of separated sodium-motile pSHU bacteria was enriched from 50% to 77.01±16.08% for 1:1 cell mix, and for the 1:9 cell mix, it was enriched from 10% to 78.56±7.47% (Fig. 3b). Thus, separation of motile bacteria for the initial cell-mixture ratio of 1:1 and 1:9 was approximately increased by 27% and 68% respectively (Fig 3b).

Numerical simulation:

We performed numerical simulations of our device to examine the diffusive spread of Na^+ ions, motile, and non-motile cells. We approximated bacterial swimming as active diffusion, with diffusion coefficients of 8.3 x 10^{-10} m^2/s (Na^+), 5.32 x 10^{-11} m^2/s (pSHU), 2 x 10^{-12} m^2/s (pSHOT), and 4.58 x 10^{-10} m^2/s (swim-locked) for Na^+ ion (15), motile bacteria , non-motile bacteria, and swim-locked bacteria (16) respectively. The origin of the coordinate-space was defined as the midpoint of channel length and width (Fig 1) and diffusive mass fraction was measured over the entire channel width (Fig 4). This mass fraction was further used to assess the profile across the channel at the inlet and outlet (at the distance of x = ±10.09 mm) to determine the separation at the divergence point, that is, the theoretical separation efficiency between outlet 1 and outlet 2.

Our simulation showed that Na^+ ions diffused further across the interface than all types of bacteria during operation (Fig. 4), as expected from diffusion input parameters. In our experiments we flowed 85 mM sodium into flowed into inlet 1 (Fig 4A, top), and from simulation in our flow conditions we calculated the sodium concentration at the midpoint of the channel (x = 0.00 mm, y = 0.00 mm) to be 39 mM. Thus, ~3 mm across the interface, in the center of the channel, roughly half the sodium concentration is available to energize stators in cells to drive active diffusion.

Comparative bacterial diffusivity, proportional to the relative diffusion coefficients, was observed for motile pSHU and non-motile pSHOT bacteria (Fig 4b). The separation efficiency for the simulation was calculated using the ratio of mass fraction at the outlet point (x = +10.09 mm, y = + 0.03 mm). The separation efficiency of motile pSHU cells calculated from the simulation was 28 times greater than the simulation separation efficiency for non-motile pSHOT bacteria, in close agreement with the separation efficiency from our experimental data i.e., 30 times.

Discussion

There exist many microfluidics device for separating and sorting motile bacteria with high precision, accuracy, and efficiency according to various taxes (6). However, many of those devices are fabricated using expensive microfabrication techniques which require sophisticated clean room facilities. Here we developed a simple and cost-effective microfluidic device using sellotape and PDMS, and Arduino powered syringe pumps with stability of laminar flow (R_e = 0.17) comparable to the other Arduino-based 3D printed syringe pumps (12).

We preferred to use pulling displacement to exert better control over the splitting of laminar flow at the outlets. Fluidic flow maintained via syringe pump can suffer from pressure drop (pulsation) along the channel. To reduce this, inlets were arranged with upright reservoirs of solution to impose hydrostatic pressure which acted as a pressure feedback system to minimize pulsation or pressure drop inside the channel. Although the separation efficiency was less than 1%, our microfluidics device was driven at comparatively high flow rates (14) to reduce residence time and select for motile bacteria, and reduce the number of non-motile bacteria that cross-contaminate our outlet 2 sample (through advection with flow).

Our device can be used to make a bulk measurement of motility in terms of the number of bacteria that separate to outlet 2. However, there already exist high throughput microscopic techniques such as Differential Dynamic Microscopy (DDM) to measure the swimming speed of motile bacteria in a sample (17). Our system offers the advantage that we can select in-line from a liquid culture and which can be employed not only to characterize the motility of bacteria but also to separate, collect,

and harvest motile bacteria. Furthermore, our approach opens the possibility to recirculate the collected bacteria through the device till the point where we obtain the bacteria with highest degree of motility. This recirculation approach could be further improved for long-term high-throughput screening of bacteria for applications in the directed evolution of motility.

Motile bacteria under the influence of flow tend to drift away from the flow direction due to helical motion of bacterial flagellar motor (18). Inside the rectangular microchannel, motile bacteria shows this drift both in the bulk fluid (rheotaxis) and upon interaction with nearby the channel surfaces (19). Based on these tendencies to divert or drift from the flow direction, motile bacteria can be difficult to separate using laminar flow-based microfluidics. For example, bacteria may get separated due to advection of fluid flow rather than diffusion. Estimations of Peclet number for motile bacteria at our flow rates (P_e = 26310) (20) showed that the bacterial sample flown through the channel length of our device (i.e., 20 mm) would only separate due to advection of fluid flow after the bacteria travels 26,310 times the channel width (1 mm) i.e., approximately 26 meter long. This agreed with our observation that we were not able to collect cells at outlet 2 when we ran both inlets in sodium-free solution (SI Fig. 3). Our separation efficiency could be increased by reducing the flow rates (14) or/and generating concentration gradient of chemoattractants or chemorepellents to induce chemotactic drift (13), however this may interfere with the stability of the laminar flow.

We showed that sodium-sensitive motile bacteria could be selectively separated even from the bacterial population even when suspended in sodium-free media. Diffused sodium ions were able to power BFM rotation and induce motility in bacteria to then select for these motile bacteria at outlet 2. It is thus possible to use a similar approach to select for diverse bacterial species from mixed or unknown samples to screen for those cells that require alternative ions for motility such as potassium (21) or even calcium (22). As the separation efficiency of the device is correlated with ion concentration, we can adjust ion composition and flow rate, and even alternate environmental conditions, to select for novel bacteria powered by rare or unusual ions. We can also use this approach to alternate ion sources to screen for bet-hedging bacteria (23) that may be optimized to dual-power

We enriched the collected bacterial species with high fraction of motile bacteria from the mixed populations of motile and non-motile bacteria. To measure this enrichment, we used the bacterial strains transformed with plasmid encoding fluorescent protein (DsRed.T4 and EGFP). Fluorescence markers are routinely used in fluorescence activated cell sorting (FACS) to separate bacteria which are tagged with respective fluorescent dye/protein (24). Here we used overnight culturing and fluorescent plate readers to distinguish the proportion of colonies of each type that were viable when culturing the volume taken from outlet 2.

We avoided using bacteria tagged with fluorescent protein in the bacterial flagellar motor as it has shown to affect the swimming speed of bacteria (25), and would not be expressed at high copy number for low resolution detection. Bacterial populations, even those generated from a single colony, can show heterogenous phenotypes, including motility (26), and indeed we observed a fraction of cells with no fluorescence, yet which we confirmed were still motile (SI Fig 3). We hypothesize this is due to the long maturation time required to properly fold dsRed to become fluorescence (27). This also confounded attempts to use direct fluorescence measurements such as fluorescent intensity, as the overall intensity of a liquid volume was dependent on the amount of dsRed in the cytoplasm of the cells, which did not necessarily accurately reflect the number of motile cells in a liquid volume. The differently tagged cells also have differential growth rates (SI Fig3). This could explain the difference in colony size between small-sized colonies of non-motile green pSHOT bacteria and larger colonies of motile red pSHU bacteria (SI Fig. 3). This visual phenotypic difference could be used to verify pSHU vs pSHOT colony assignment during colony counting to determine the enrichment ratios in our experiments.

Separation efficiency measured from simulation data of motile pSHU and non-motile pSHOT bacteria showed that motile pSHU diffused 28 times more than non-motile. This simulated separated efficiency data agreed with our experimental data (i.e., 30 times more for pSHU compared to pSHOT). This small discrepancy could arise from a few small differences: our experimental measurements to detect viable cells, not all cells, so we would expect our measurements to be lower. We will also lose some cells to surface coating of the tubing, and containers used in dilution and subsequent culturing. Besides, bacterial swimming may deviate from strictly diffusive behavior [ref], and the flow in our device is likely further from ideal behaviour close to the outlets. What simulations do provide is a comparison between the diffusivity of the energy source (sodium ions), and attractants, in comparison with the diffusive capacity of motile and non-motile cells, and also provides a mechanism to refine designs and geometries for specific applications in bacterial selection and separation.

Conclusions

Our system can be rapidly prototyped and can separate small differences in diffusivity by tweaking flow rates and channel geometry for optimization of specific applications in micron-scale separation. In this paper, we fabricated a cheap, effective microfluidics system for separation and enrichment of sodium-powered motile bacteria from non-motile populations. Our system has broad applications in environmental and field screening of bacterial species from liquid, as well as for quick assays to test the bulk motility of a sample. We envision future applications in directed and experimental evolution, particularly where these fields intersect with the evolution and adaptation of bacterial motility. That said, this device is equally translatable for applications in other systems where micron-scale motility is of importance, such as in the separation of motile eukaryotes (such as sperm for fertility applications, or cilia) and the multiple motile archaea strains (powered by the archaellum) that are increasingly of interest in studies in convergent evolution and for harvesting novel biotechnology.

Materials and methods

3D printed custom-built syringe pump

Our custom-built syringe pump comprised of two 1 mL syringes in 3D printed syringe holders, two 28BYJ-48 (5V DC) stepper motors, an Arduino UNO R3 board, and an Adafruit Motorshield V2. Syringe adaptors were connected to the microfluidic chip using PTFE tubing (BOLA Inc.) with internal diameter (ID) of 0.5 mm and outer diameter (OD) of 1 mm. The stepper motors were connected to M1, M2, and M3, M4 ports on the Adafruit Motorshield V2 (Arduino UNO R3) and placed on the 3D printed syringe holder (Fig. 1). A program based on C/C++ language was scripted to run two stepper motors at two independent rates simultaneously in the order of few hundreds of uL/min. The program code is presented in Supplementary information.

Fabrication of microfluidics device

Y-shaped channel was designed using a CAD drawing tool, Fusion360 and the sketch was exported in .dxf file format to make it executable in a tape cutter (Silhouette Curio, USA). Brown adhesive tape was laminated on the glass slide (75mm by 25mm), baked in an oven at 65 ^{o}C for 30 min, and cooled down to room temperature after gentle roll over the tape (removes air bubbles if present). The channel mould was cut on the slide using a tape cutter (Silhouette Curio, USA) and the excess tape outside of the channel structure was removed. Then, glass slide engraved with Y-shaped channel mould was placed in 3D-printed rectangular casket using tape (checked if the interfaces were tightly sealed well to prevent the leakage of PDMS), 10 g Clip-pack PDMS mix (SYLGARD®184) was poured into the casket, and left in vacuum for degassing. PDMS was cured in oven at 65°C for 2 hours (or overnight). Cured PDMS was cut using scalpel and removed from the mould. Holes were punched

at inlets and outlets using 0.75 mm biopsy punch (EMS/Rapid-core). Surfaces of PDMS cast and glass slide were treated with plasma discharge for 3 minutes and instantly bonded together with a slight press. Finally, microfluidics channel was treated with sterile 1% BSA solution (prepared in Milli-Q water) to prevent cell adhesion and stored at room temperature for future use.

Image analysis of laminar-flow stability

Red dye was used to test the laminar flow stability inside the microfluidic channel. Initially, and at 30 min intervals during the microfluidics run, 5-minute video was recorded using Olympus inverted microscope at the magnification of 4X objective lens using ToupView imaging software. This 5-minute video was rendered to extract stack of image sequences using Photoshop (Adobe Inc.). Then, the image sequences were processed and analysed using Fiji (Image J) software to determine the laminar flow stability (12). For this, a rectangular region of interest (ROI) was defined and cropped for a single image. Then, the contrast of cropped image was enhanced by 0.5%, black background was subtracted, converted to binary mask, and the area-fraction of red dye was measured. Ultimately, this operation for a single image was executed to a complete directory (other image sequences).

Bacterial sample preparation

Plasmid pSHU1234 is based on pBAD33 backbone for expression of sodium-powered stator units; PomA and PotB whereas plasmid pSHOT is pSHU1234 but with complete deletion of PotB and partial deletion at the C-terminal of PomA from amino acid residue 203 to 254 (28). These plasmids were transformed into *E coli* strain RP6894; Δ(motA-motB) to obtain the bacterial strains of two different types, one with plasmid pSHU1234 (contains PomA and PotB encoding gene; thus, are motile in sodium ion) and the other strain with plasmid pSHOT (ΔPomA; thus, non-motile). Furthermore, these strains were co-transformed with plasmids, encoding fluorescent protein for fluorescence experiment. Bacterial strain pSHU1234 was transformed with DsRed.T4 plasmid (encodes red fluorescent protein) whereas pSHOT with pACGFP1 plasmid (encodes green fluorescent protein) (13).

Approximately 4-5 colonies were picked from bacterial agar plates and inoculated into the LB broth. Then the culture was incubated in rotary shaker at 37°C for 2 hours (normally bacterial O.D. at 600 nm reaches the value > 0.5 after this time of incubation). Bacterial culture was centrifuged at 7000 rpm for 3 minutes, washed at least three times with water and finally suspended in motility buffer (10 mM KPi (pH 7.0), 85 mM NaCl, 0.1 mM EDTA-Na). Bacterial sample was resuspended in 1 mL volume to obtain the O.D. value between 0.5 – 0.6, and motility was checked under microscope before running inside microfluidics device.

Operation of microfluidics device

500 uL of motility buffer or water was pushed into the channel till the solution reached the certain height in the reservoirs (inlet 1 and inlet 2). The device with prefilled solution was degassed in vacuum for around two hours to gets rid of air bubbles. Before loading the sample, 300 uL of the solution was pulled out of the device which results the stage where the inlet reservoirs are emptied (also helps to check the clogging inside channels). One of the reservoirs was loaded with red dye or bacterial sample and the other with solution such as motility buffer or water. Bacteria were collected from respective outlets, serially diluted, and 10 µL droplets were placed in the agar plate for colony count (Fig. 3a) (29). Here,

separated fraction of motile bacteria was calculated as a ratio of bacterial count from outlet 2 and total bacterial count from outlet 1 and outlet 2 (14).

Numerical simulation

Computational Fluid Dynamics (CFD) simulations were conducted to verify the performance of the microfluidic system and demonstrate the active diffusion of sodium, motile and non-motile bacteria in the device. In the simulations, the mediums were assumed to be an isothermal liquid, viscous, incompressible, and Newtonian fluids. Physical properties of the mediums are constant and unaffected by the channel geometry. The flow regime is laminar, and the gravity effects on the flow field are negligible.

Figure 1(b) shows the geometry used in this simulation and the Cartesian coordinate system that was placed in the center of channel length and width (red dot, Fig 1b). A uniform inlet velocity was set at the inlet boundary condition, and flow rate weighting of 1:2 (Outlet-2/Outlet-1) was placed at the outlet boundary condition. A no-slip boundary condition, where the velocity is zero, was applied at the walls in the computational geometry. The multi-zone quadrilateral-triangle computational mesh was generated in this domain using the pre-processor ANSYS Meshing software. The maximum mesh size used was 5 µm, and it is chosen based on a mesh independency analysis. No significant difference was observed in the simulations when the mesh was refined.

The computational platform used for the simulations was Fluid Flow (FLUENT) package of ANSYS (ANSYS Inc., 2019). For the isothermal flow of a Newtonian fluid of constant density, the governing equations were developed as incompressible Navier–Stokes equations, including momentum equation, and continuity equation. To include the species transport based on the concertation gradient in the diffusion-dominated laminar flow, the Maxwell-Stefan equations were used to find the diffusive mass fraction. The high degree Pressure-Implicit with Splitting of Operators (PISO) was used for pressure velocity coupling, and the PRESTO (Pressure Staggering Option) algorithm was employed for the pressure interpolation. The second-order upwind differencing and the Least Square Cell-Based gradient method was used for solving transport equations and the spatial discretization, respectively. The transient flow condition with bounded second-order implicit formulation was considered for simulation to monitor the flow within the device over time until it gets to the steady-state condition. The time step for the integration used is 10^{-6} second. In each time step, a maximum of 20 iterations was found to be sufficient for convergence, and the absolute convergence criterion was set to 10^{-4}.

The numerical simulations were carried out on a DELL Precision Tower having two processors of "Intel Xeon CPU E5-2699 V4", including 25 physical cores with the maximum speed of 2.6 GHz for an individual core and 256 GB memory.

Authors contribution statement

JY designed and executed fluidics, cell culturing and fluorescence experiments, and wrote the manuscript. MNK executed simulations. SA designed, wrote, and tested code to drive Arduino. MG designed experiments and wrote the manuscript. MABB supervised the project, designed, and executed experiments, and wrote the manuscript.

Conflict of interest

There are no conflicts to declare.

Acknowledgements

We would like to acknowledge the gift of a 3D printed holder for the syringe pumps and a test Arduino from Dr James Walsh and A/Prof Till Boecking from the Centre for Single Molecule Science, UNSW Sydney. We also would like to thank Prof. Wenbin Du from the Institute of Microbiology at the Chinese Academy of Sciences, Beijing, for the plasmid encoding for fluorescent proteins used in this work. This work was conducted (in part) using the 'Design House' facilities at the South Australia node of the Australian National Fabrication Facility (ANFF-SA), a company established under the National Collaborative Research Infrastructure Strategy to provide nano- and micro-fabrication facilities for Australia's researchers.

References

1. Raina J-B, Fernandez V, Lambert B, Stocker R, Seymour JR. The role of microbial motility and chemotaxis in symbiosis. Nature Reviews Microbiology. 2019 May;17(5):284–94.

2. Häse CC, Barquera B. Role of sodium bioenergetics in Vibrio cholerae. Biochimica et Biophysica Acta (BBA) - Bioenergetics. 2001 May 1;1505(1):169–78.

3. Lai Y-W, Ridone P, Peralta G, Tanaka MM, Baker MAB. Evolution of the Stator Elements of Rotary Prokaryote Motors. Journal of Bacteriology [Internet]. 2020 Jan 15 [cited 2020 Nov 5];202(3). Available from: https://jb.asm.org/content/202/3/e00557-19

4. Micali G, Endres RG. Bacterial chemotaxis: information processing, thermodynamics, and behavior. Current Opinion in Microbiology. 2016 Apr 1;30:8–15.

5. Scheler O, Postek W, Garstecki P. Recent developments of microfluidics as a tool for biotechnology and microbiology. Current Opinion in Biotechnology. 2019 Feb 1;55:60–7.

6. Gurung JP, Gel M, Baker MAB. Microfluidic techniques for separation of bacterial cells via taxis. Microb Cell. 7(3):66–79.

7. Altegoer F, Schuhmacher J, Pausch P, Bange G. From molecular evolution to biobricks and synthetic modules: a lesson by the bacterial flagellum. Biotechnology and Genetic Engineering Reviews. 2014 Jan 2;30(1):49–64.

8. Chiu FWY, Stavrakis S. High-throughput droplet-based microfluidics for directed evolution of enzymes. ELECTROPHORESIS. 2019;40(21):2860–72.

9. Gupta V, Sengupta M, Prakash J, Tripathy BC. Immunology and Medical Microbiology. Basic and Applied Aspects of Biotechnology. 2016 Oct 23;167–90.

10. Morgan AJL, Jose LHS, Jamieson WD, Wymant JM, Song B, Stephens P, et al. Simple and Versatile 3D Printed Microfluidics Using Fused Filament Fabrication. PLOS ONE. 2016 Apr 6;11(4):e0152023.

11. Weisgrab G, Ovsianikov A, Costa PF. Functional 3D Printing for Microfluidic Chips. Advanced Materials Technologies. 2019;4(10):1900275.

12. Lake JR, Heyde KC, Ruder WC. Low-cost feedback-controlled syringe pressure pumps for microfluidics applications. PLOS ONE. 2017 Apr 3;12(4):e0175089.

13. Dong L, Chen D-W, Liu S-J, Du W. Automated Chemotactic Sorting and Single-cell Cultivation of Microbes using Droplet Microfluidics. Scientific Reports. 2016 Apr 14;6(1):24192.

14. Ishikawa T, Shioiri T, Numayama-Tsuruta K, Ueno H, Imai Y, Yamaguchi T. Separation of motile bacteria using drift velocity in a microchannel. Lab Chip. 2014 Feb 4;14(5):1023–32.

15. Johnson KS. The calculation of ion pair diffusion coefficients: A comment. Marine Chemistry. 1981 Apr 1;10(3):195–208.

16. Wu M, Roberts JW, Kim S, Koch DL, DeLisa MP. Collective Bacterial Dynamics Revealed Using a Three-Dimensional Population-Scale Defocused Particle Tracking Technique. Appl Environ Microbiol. 2006 Jul;72(7):4987–94.

17. Martinez VA, Besseling R, Croze OA, Tailleur J, Reufer M, Schwarz-Linek J, et al. Differential Dynamic Microscopy: A High-Throughput Method for Characterizing the Motility of Microorganisms. Biophysical Journal. 2012 Oct 17;103(8):1637–47.

18. Jing G, Zöttl A, Clément É, Lindner A. Chirality-induced bacterial rheotaxis in bulk shear flows. Science Advances. 2020 Jul 1;6(28):eabb2012.

19. Lauga E. Bacterial Hydrodynamics. Annual Review of Fluid Mechanics. 2016;48(1):105–30.

20. Fuller NJ, Licata NA. Numerical and analytical approaches to an advection-diffusion problem at small Reynolds number and large P\'eclet number. arXiv:160909366 [physics] [Internet]. 2017 Aug 31 [cited 2020 Nov 24]; Available from: http://arxiv.org/abs/1609.09366

21. Naganawa S, Ito M. MotP Subunit is Critical for Ion Selectivity and Evolution of a K+-Coupled Flagellar Motor. Biomolecules. 2020 May;10(5):691.

22. Ito M, Takahashi Y. Nonconventional cation-coupled flagellar motors derived from the alkaliphilic Bacillus and Paenibacillus species. Extremophiles. 2017 Jan 1;21(1):3–14.

23. Beaumont HJE, Gallie J, Kost C, Ferguson GC, Rainey PB. Experimental evolution of bet hedging. Nature. 2009 Nov 5;462(7269):90–3.

24. Liao X, Makris M, Luo XM. Fluorescence-activated Cell Sorting for Purification of Plasmacytoid Dendritic Cells from the Mouse Bone Marrow. J Vis Exp [Internet]. 2016 Nov 4 [cited 2020 Nov 13];(117). Available from: https://www.ncbi.nlm.nih.gov/pmc/articles/PMC5226086/

25. Heo M, Nord AL, Chamousset D, van Rijn E, Beaumont HJE, Pedaci F. Impact of fluorescent protein fusions on the bacterial flagellar motor. Scientific Reports. 2017 Oct 3;7(1):12583.

26. Salek MM, Carrara F, Fernandez V, Guasto JS, Stocker R. Bacterial chemotaxis in a microfluidic T-maze reveals strong phenotypic heterogeneity in chemotactic sensitivity. Nature Communications. 2019 Apr 23;10(1):1877.

27. Balleza E, Kim JM, Cluzel P. Systematic characterization of maturation time of fluorescent proteins in living cells. Nat Methods. 2018 Jan;15(1):47–51.

28. Ishida T, Ito R, Clark J, Matzke NJ, Sowa Y, Baker MAB. Sodium-powered stators of the bacterial flagellar motor can generate torque in the presence of phenamil with mutations near the peptidoglycan-binding region. Molecular Microbiology. 2019;111(6):1689–99.

29. Naghili H, Tajik H, Mardani K, Razavi Rouhani SM, Ehsani A, Zare P. Validation of drop plate technique for bacterial enumeration by parametric and nonparametric tests. Vet Res Forum. 2013;4(3):179–83.

Figures

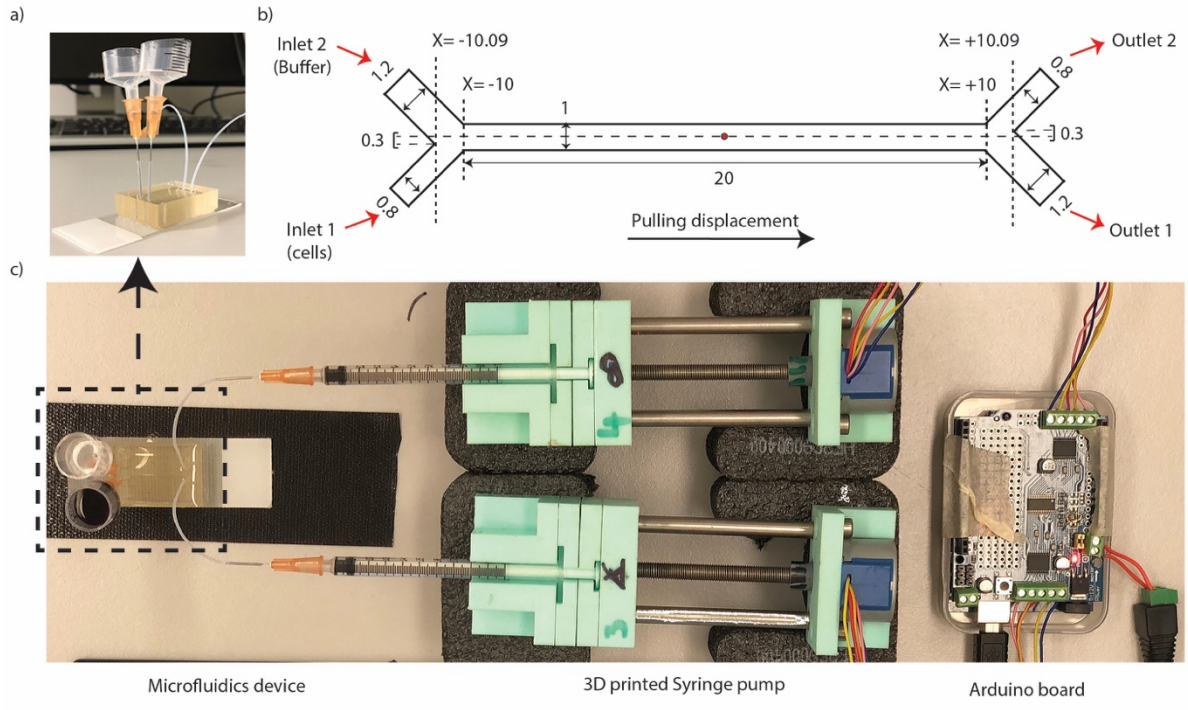

Figure 1: Fabrication of microfluidic device. a) Photo image of microfluidic device with upright reservoirs. b) schematics diagram of asymmetric Y-shaped channel. c) Photo image of microfluidic platform containing Arduino board, custom-built 3D printed syringe pumps, and microfluidics device.

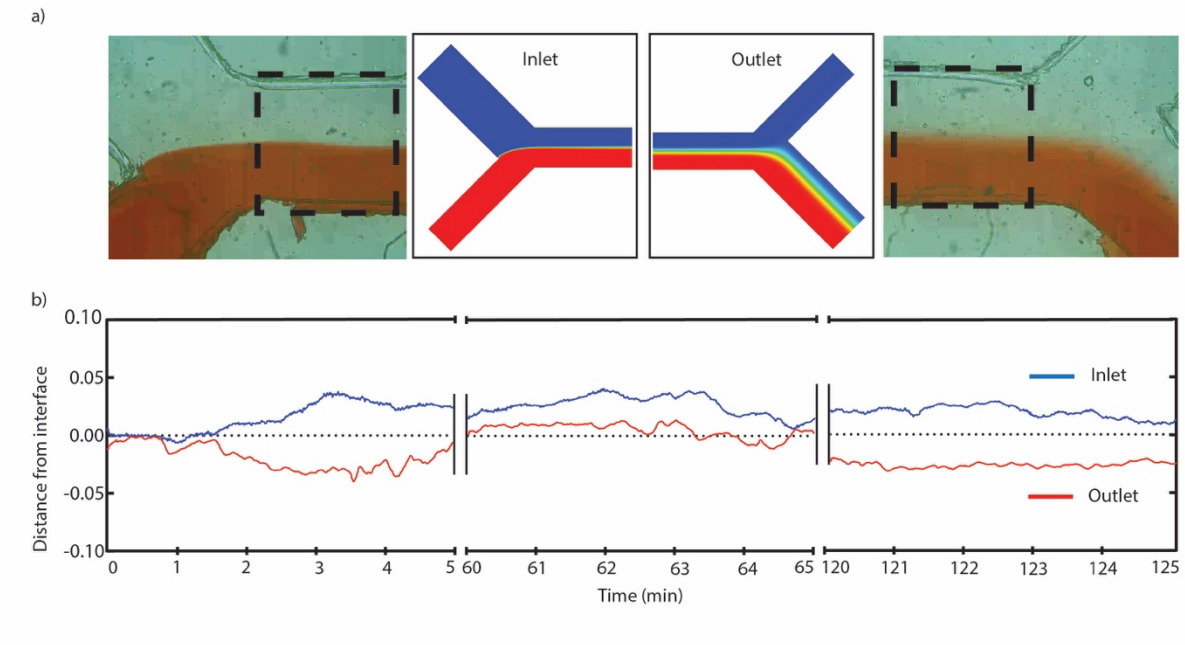

Figure 2: Characterization of microfluidic device. a) Laminar flow generated using our microfluidic device; represented by red dye (bottom) and colorless solution (water, top) streams in inlet (left) and outlet (right). Adjacent is numerical simulations for ion diffusion matched at inlet and outlet (see Fig 4). b) Line graph showing laminar interface fluctuation from center (0.00) over five-minute intervals to measure flow stability at 0 min, 60 min, and 120 min (plot of relative distance from interface vs time in minutes).

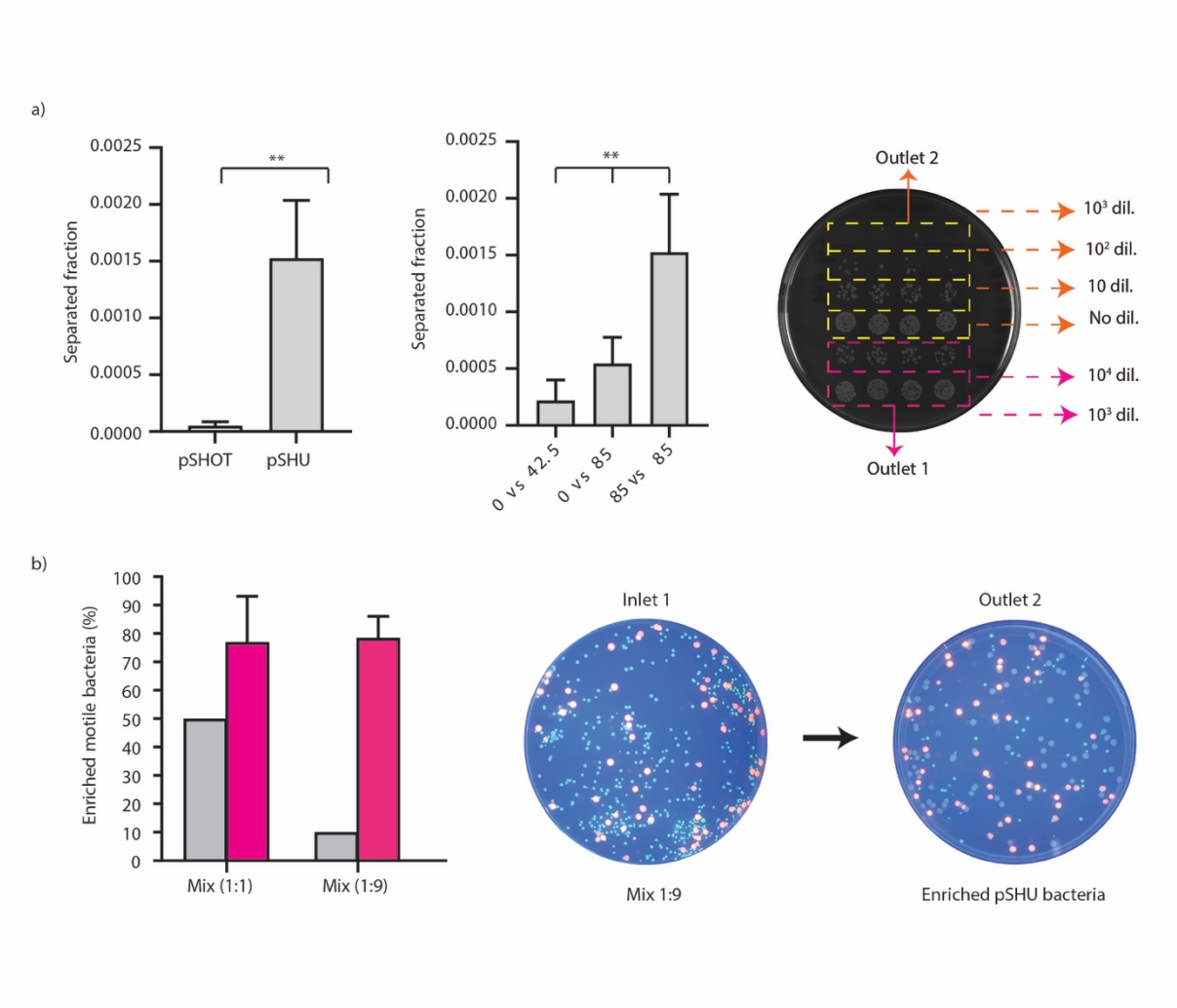

Figure 3: Separation and enrichment of sodium-motile bacteria. Inlet samples are configured as per Fig. 1. a) Left – separation of motile pSHU bacteria and non-motile pSHOT bacteria, suspended in motility buffer containing 85 mM of NaCl and run against the solution of motility buffer containing 85 mM NaCl, Middle – selection of motile pSHU bacteria, suspended in 0 mM of NaCl versus varying concentration of sodium (42.5 mM and 85 mM of NaCl), and Right – droplet method to count bacterial colony collected from outlet 1 with no dilution, 10, and 10^2 dilutions whereas outlet 2 with 10^3 and 10^4 dilutions. b) Left - % of enriched motile pSHU bacteria for two different mixtures of fluorescent cells in inlets (pSHU:pSHOT; 1:1 and 1:9), Middle – Spread plate of fluorescent cell mix ration of 1:9 (10^4 diluted) subjected into inlet 1 of microfluidic device, and Right – Spread plate of 100 uL collected cells from outlet 2 after separation (No dilution).

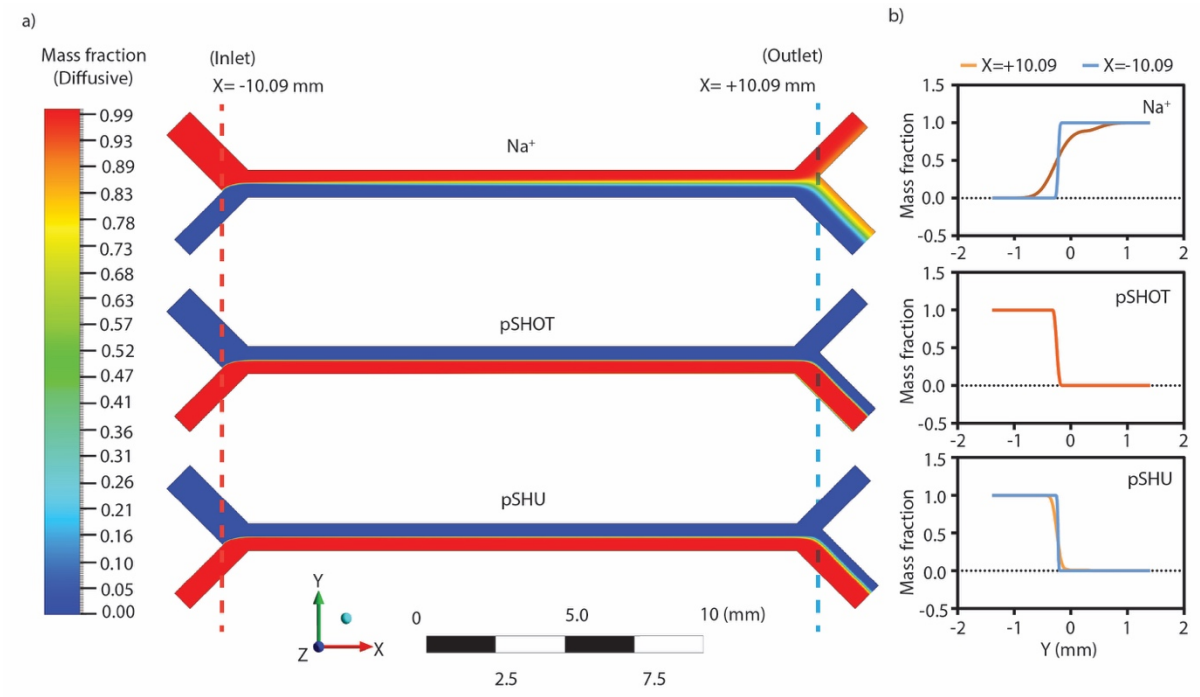

Figure 4: Numerical simulation using ANSYS Fluent software. a) (top to bottom) - image of simulation showing diffusion gradient of sodium ions, non-motile pSHOT, and motile pSHU. b) (Top to bottom) – Line graph of diffusive mass fraction vs distance in Y-axis (mm) for sodium ions, non-motile pSHOT, and motile-pSHU at the x-coordinate of ±10.09 mm from simulated data.